Journal of Solid State Chemistry 183 (2010) 1083–1089

Contents lists available at ScienceDirect

Journal of Solid State Chemistry

journal homepage: www.elsevier.com/locate/jssc

Effects of the *A*-site cation number on the properties of $Ln_{5/8}M_{3/8}MnO_3$ manganites

J.A. Collado [a], J.L. García-Muñoz [b], M.A.G. Aranda [a,*]

[a] Departamento de Química Inorgánica, Universidad de Málaga, 29071 Málaga, Spain
[b] Instituto de Ciencia de Materiales de Barcelona, CSIC, Campus de Bellaterra, 08193 Bellaterra, Barcelona, Spain

ARTICLE INFO

Article history:
Received 27 October 2009
Received in revised form
9 January 2010
Accepted 9 March 2010
Available online 15 March 2010

Keywords:
Variance
DSC
Phase separation
Manganites

ABSTRACT

The properties of manganites can be tuned by changing the doping level x in $Ln_{1-x}M_xMnO_3$. A second mechanism allows tuning of magnetic and electronic properties, for fixed x values, by varying the average *A*-cation radius, $\langle r_A \rangle$. Moreover, for fixed x and $\langle r_A \rangle$ values, the changes in the *A*-cation size variance, σ^2, also modify the ferromagnetic and metal–insulator transition temperatures. Here, we investigate the influence of the number of *A*-site cations on $Ln_{5/8}M_{3/8}MnO_3$ manganites, where x, $\langle r_A \rangle$ and σ^2 values are kept constant, and in the absence of phase separation phenomena. We have found that the number of cation species at the *A* site (N_A) has a strong influence on the width of the ferromagnetic and metal–insulator transitions, and a small influence on the average transition temperature. This behavior is opposite to that observed for increasing values of the variance σ^2 in manganites, with the same x and $\langle r_A \rangle$ values, where average transition temperatures are strongly reduced.

1. Introduction

The electronic and magnetic properties of rare earth manganites, $Ln_{1-x}M_xMnO_3$ (*Ln*=rare earth, *M*=alkaline earth), have been widely studied [1–3]. Besides colossal magnetoresistance (CMR), charge ordering, orbital ordering and different types of ordered magnetic phases, some manganites exhibit phase separation phenomena at different length scales [4]. These properties, and the different types of electronic, conducting, structural and magnetic transitions, are commonly very sensitive to chemical or physical modifications and can be easily tuned by different methods.

The main and most commonly used strategy to vary the physical properties of manganites is to play with the charge carrier concentration. Changing the doping level x in $Ln_{1-x}M_xMnO_3$, the Mn^{3+}/Mn^{4+} ratio can be modulated and, hence, the charge carrier concentration. Archetypal examples of this type of studies are the $La_{1-x}Sr_xMnO_3$ [5–8] and $La_{1-x}Ca_xMnO_3$ [9,10] series. A second mechanism allows changing of electronic and magnetic properties, for fixed x values, that consists in varying the size of the atoms at the *A* site of the perovskite (average radius, $\langle r_A \rangle$, of the *A* cations) in stoichiometries like $(Ln^1_{1-y}Ln^2_y)_{1-x}(M)_xMnO_3$ or $(Ln)_{1-x}(M^1_{1-z}M^2_z)_xMnO_3$ (*Ln*=rare earth, *M*=alkaline earth). Thus, the astonishing behavior of paradigmatic series such as $La_{5/8-y}Pr_yCa_{3/8}MnO_3$, $La_{0.70-y}Pr_yCa_{0.30}MnO_3$ or $Nd_{0.7}Sr_{0.3-y}Ca_yMnO_3$ has been extensively studied during recent years [11–20]. A third mechanism for fixed x and $\langle r_A \rangle$ values that produces changes in the physical response relies on the disparity or mismatch of individual *A* cation radii (*A*-site cation disorder) [21]. The mismatch associated with different cation types at the same crystallographic position is parameterized using the *A*-cation size variance, $\sigma^2=(\sum \chi_i r_i^2 - \langle r_A \rangle^2)$, where χ_i is the fractional occupancy of the *A* site and r_i the corresponding ionic radii [22]. Specific effects attributed to increasing values of σ have been reported in several series of perovskites. Some examples can be found in Refs. [22–28].

The influence of *A*-cation size variance and correlation between σ^2 and magnetotransport properties in $Ln_{5/8}M_{3/8}MnO_3$ series with $\langle r_A \rangle = 1.204$ Å (kept constant) was already reported by us [29]. All samples (3×10^{-4} Å$^2 \le \sigma^2 \le 71\times10^{-4}$ Å^2) showed ferromagnetic-to-paramagnetic (FM–PM) and metal-to-insulator (M–I) transitions, and the temperatures T_C and T_{MI} show a strong negative correlation with σ^2. All these samples have the orthorhombic *Pnma* structure but the lattice strain in the *ac*-plane [$S_{ac}=2(c-a)/(c+a)$] changes from positive to negative values when moving from the orbital disordered (low σ^2) to the orbital ordered (high σ^2) samples.

Although the samples with smaller variances generally exhibit sharper magnetization transitions, in the previous study [29] a systematic monotonous correspondence was not observed. In an attempt to understand this lack of a systematic monotonous correspondence, we have extended and completed the previous study by preparing and characterizing new samples within the

* Corresponding author. Fax: +34 952 13 20 00.
E-mail address: g_aranda@uma.es (M.A.G. Aranda).

0022-4596/$ - see front matter © 2010 Elsevier Inc. All rights reserved.
doi:10.1016/j.jssc.2010.03.018

$Ln_{5/8}M_{3/8}MnO_3$ family. The strategy followed in the present work is different because the new compositions have been chosen in order to obtain several sets of manganites in which the values of the three parameters x, $\langle r_A \rangle$ and σ^2, and not only the first two, are identical. The new cation stoichiometries were determined, prepared and characterized. For instance, in addition to $Nd_{5/8}Sr_{0.255}Ca_{0.12}MnO_3$ previously studied [29], $La_{0.315}Sm_{0.31}Ca_{0.175}Sr_{0.20}MnO_3$ has been prepared, because it has the same values for the three variables ($x=3/8$, $\langle r_A \rangle = 1.204$ Å and $\sigma^2 = 0.0040$ Å^2) but four different types of A cations instead of three. The magnetic and electric properties are reported as well as a calorimetric characterization and low-temperature X-ray thermodiffractometries. We report clear effects on the width of the transitions associated with the number of distinct cation types occupying the A site, but keeping unchanged x, $\langle r_A \rangle$ and σ^2. Moreover, despite the number of different cations used in many of the manganites, we have confirmed that all the solid solutions investigated did not display any signature of low-temperature phase separation. The conclusions are based on single phased but strained materials.

2. Materials and methods

2.1. Samples

We recall that Curie temperature, T_C, is maximized in $La_{1-x}Ca_xMnO_3$ series for $x=3/8$. Seven different compositions of the type $Ln_{5/8}M_{3/8}MnO_3$ with $\langle r_A \rangle = 1.204$ Å have been considered: $La_{5/8}Ca_{3/8}MnO_3$, $Pr_{5/8}Sr_{0.178}Ca_{0.197}MnO_3$, $Nd_{5/8}Sr_{0.255}Ca_{0.12}MnO_3$, $Sm_{0.504}Nd_{0.121}Sr_{3/8}MnO_3$, $La_{0.257}Nd_{0.368}Ca_{0.225}Sr_{0.15}MnO_3$, $La_{0.315}Sm_{0.31}Ca_{0.175}Sr_{0.2}MnO_3$ and $Pr_{5/8}Ca_{0.295}Ba_{0.08}MnO_3$. The first four samples are the same as those included in Ref. [29]. In order to explore the role of the number of A-site cations in these series, three new samples have been prepared (the latter three compositions) with the same average ionic radius. The A-cation size variance (σ^2) of all compounds is reported in Table 1. Two of the new compositions, $La_{0.257}Nd_{0.368}Ca_{0.225}Sr_{0.15}MnO_3$ ($\sigma^2 \times 10^4 = 25$ Å^2, $N_A=4$) and $La_{0.315}Sm_{0.31}Ca_{0.175}Sr_{0.2}MnO_3$ ($\sigma^2 \times 10^4 = 40$ Å^2, $N_A=4$) have been prepared to match the σ values of previous samples but with four different A-site cations (see Table 1). On the other hand, $Pr_{5/8}Ca_{0.295}Ba_{0.08}MnO_3$ ($\sigma^2 \times 10^4 = 62$ Å^2, $N_A=3$) has been also prepared to check the features of a sample with very large variance and three A-site cations. The ceramic method was employed to prepare the new stoichiometries by following the same procedure previously reported [29].

2.2. Powder diffraction

All samples were characterized by laboratory X-ray powder diffraction (LXRPD) at room temperature (RT) on an X'Pert Pro MPD automated diffractometer equipped with a Ge(1 1 1) primary monochromator (strictly monochromatic Cu$K\alpha_1$ radiation) and an X'Celerator detector. The overall measurement time was ~2 h per pattern to have very good statistics over the 2θ range of 20–100° at 0.017° step size. The low temperature diffraction patterns were collected between 20° and 60° (2θ) with the samples loaded in an Anton-Paar TTK 450 Low-Temperature Chamber. The patterns were collected on heating from 100 K to room temperature.

2.3. Magnetic and transport study

Magnetization and resistivity data were recorded in a Quantum Design PPMS (Physical Properties Measurement System). DC magnetization data have been recorded with an applied field of 0.1 T on heating from 5 to 300 K (field cooled). Resistivity was measured in zero field using the standard four probes method on a cooling–warming cycle at 3 K min^{-1} rate.

2.4. Calorimetric study

The calorimetric data have been obtained using differential scanning calorimetry (DSC) with computer-aided data analysis (Shimadzu DSC-50). The studied temperature range was from 300 to 110 K and the scanning rate was −5 K min^{-1}.

3. Results

3.1. Structural study

All samples reported in Table 1 are single phase crystallizing in the orthorhombic *Pnma* perovskite structure. The values of cell parameters and orthorhombic strain of the lattice in the *ac*-plane [$S_{ac}=2(c-a)/(c+a)$] are given in Table 1. It should be noticed that the series switch from the superstructure type O″ ($c>a>b/\sqrt{2}$, $S_{ac}>0$) for low variance values to O′ type ($a>c>b/\sqrt{2}$, $S_{ac}<0$) for large variance values.

3.2. Magnetization study

All samples show a FM–PM transition in the magnetization data, see Fig. 1. The magnetization data were taken with $H=0.1$ T

Table 1
Summary of chemical, structural and physical data for the $Ln_{5/8}M_{3/8}MnO_3$ series with $\langle r_A \rangle = 1.204$ Å.

Composition	$\langle r_A \rangle$ (Å)	σ^2 ($\times 10^{-4}$ Å^2)	N_A	T_C[a] (K)	ΔT_C[b] (K)	T_{MI}[c] (K)	T_C[d] (K)	ΔH (J mol^{-1})	ΔS (J K^{-1} mol^{-1})	a (Å)	b (Å)	c (Å)	S_{ac}	Ref.
$La_{5/8}Ca_{3/8}MnO_3$	1.206	3	2	269	5.7(4)	270	271	−440	−1.6	5.44781(3)	7.69370(4)	5.46164(3)	0.25	[29]
$Pr_{5/8}Sr_{0.178}Ca_{0.197}MnO_3$	1.205	25	3	237	7.4(3)	238	230	−401	−1.7	5.44231(3)	7.68862(3)	5.45267(2)	0.19	[29]
$La_{0.257}Nd_{0.368}Ca_{0.225}Sr_{0.15}MnO_3$	**1.205**	**25**	**4**	**235**	**29.8(4)**	**243**	**233**	**−227**	**−1.0**	**5.4459(3)**	**7.6969(5)**	**5.4509(4)**	**0.09**	**t.w.**[e]
$Nd_{5/8}Sr_{0.255}Ca_{0.12}MnO_3$	1.204	40	3	197	6.9(4)	201	190	−359	−1.9	5.44516(2)	7.68826(2)	5.44649(2)	0.02	[29]
$La_{0.315}Sm_{0.31}Ca_{0.175}Sr_{0.2}MnO_3$	**1.204**	**40**	**4**	**184**	**30.1(5)**	**199**	**181**	**−259**	**−1.4**	**5.4483(9)**	**7.6916(9)**	**5.4518(9)**	**0.06**	**t.w.**
$Pr_{5/8}Ca_{0.295}Ba_{0.08}MnO_3$	**1.206**	**62**	**3**	**122**	**16.5(6)**	**124**	**115**	**−142**	**−1.2**	**5.4520(4)**	**7.6883(6)**	**5.4473(4)**	**−0.09**	**t.w.**
$Sm_{0.504}Nd_{0.121}Sr_{3/8}MnO_3$	1.203	71	3	130	26.0(6)	139	–	–	–	5.44695(4)	7.68555(4)	5.44505(3)	−0.03	[29]

[a] Curie transition temperature from the magnetization study on heating determined from a Lorentzian function fit of the derivative curves.
[b] Width of the magnetization transition.
[c] MI transition temperature from the resistivity study on heating.
[d] Transition temperature from the DSC study on heating.
[e] Samples prepared for this work are highlighted in bold.

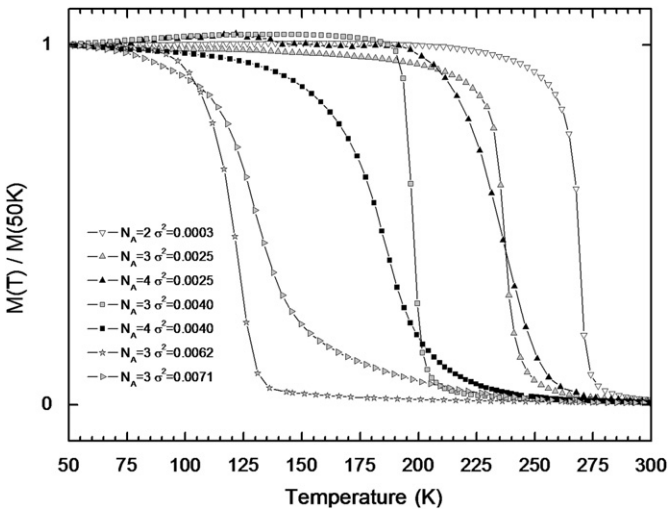

Fig. 1. Magnetization versus temperature curves, on heating, for the $Ln_{5/8}M_{3/8}MnO_3$ $\langle r_A \rangle = 1.204$ Å series (cooled under 0.1 T field). The $\sigma^2 \times 10^4/Å^2$ values are labeled.

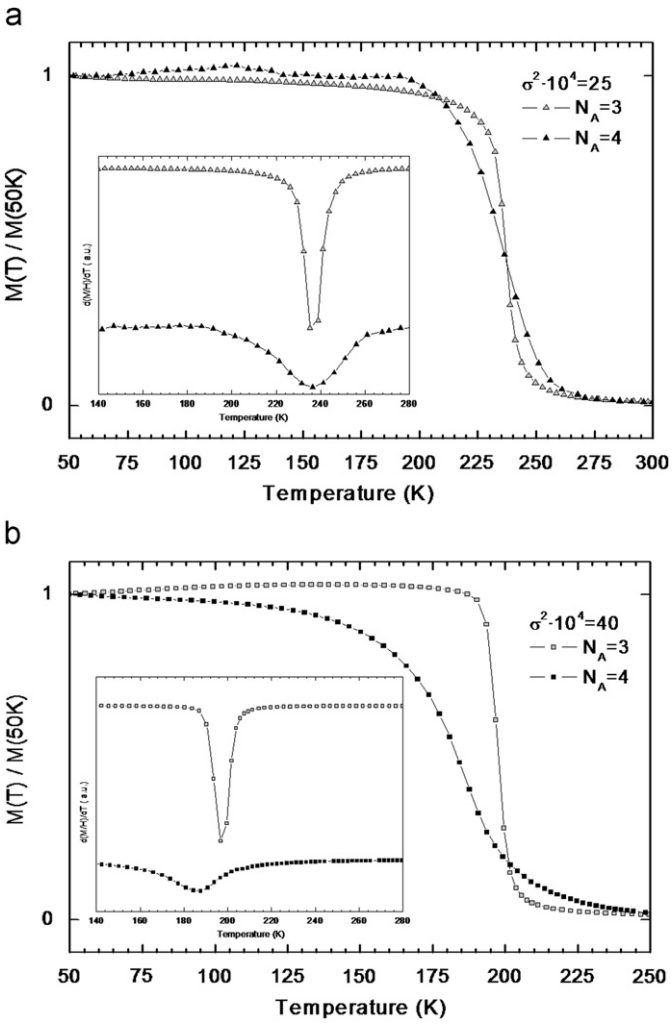

Fig. 2. Magnetization data normalized at 50 K for compositions with (a) $\sigma^2 = 0.0025$ Å^2 and $N_A = 3, 4$ and (b) $\sigma^2 = 0.0040$ Å^2 and $N_A = 3, 4$. The inset highlights the widths of the transitions by plotting $dM(T)/dT$.

(field cooled measurements). The characteristic Curie temperatures (T_C values) were determined using the temperature derivatives of the magnetization/field ($d(M/H)/dT$). A detailed comparison of the magnetization data for the phases with $\sigma^2 = 0.0025$ and 0.0040 Å^2 are given in Fig. 2(a) and (b), respectively. The peaks in the derivative curves have been fitted with Gaussian and Lorentzian functions to obtain the T_C values and the transition widths (full width at half maximum, ΔT_C). The goodness of the fits is invariably better using the Lorentzian function. T_C and ΔT_C values obtained from these (Lorentzian) fits are given in Table 1.

3.3. Resistivity study

The resistivity curves for four selected samples, those with $\sigma^2 = 0.0025$ and 0.0040 Å^2 and $N_A = 3$ and 4, are displayed in Fig. 3 (normalized at room temperature, obtained on heating). All samples undergo a low temperature metal-to-insulator (M–I) transition, and the transition temperatures T_{MI} reported in Table 1 have been taken from the maxima in the $\rho(T)$ curves during the heating process.

3.4. Calorimetric study

Fig. 4 shows raw DSC data for $\sigma^2 = 0.0025$ Å^2 ($N_A = 3$ and 4 samples) on a cooling–heating cycle. Fig. 5 shows similar raw DSC data for $\sigma^2 = 0.0040$ Å^2 ($N_A = 3$ and 4). The corresponding curves for $\sigma^2 = 0.0062$ Å^2 ($N_A = 3$) are shown in Fig. 6. The transition is endothermic on heating ($\Delta H > 0$) and the hysteresis is small in all cases. The enthalpy and entropy changes (ΔH and ΔS) and the T_C

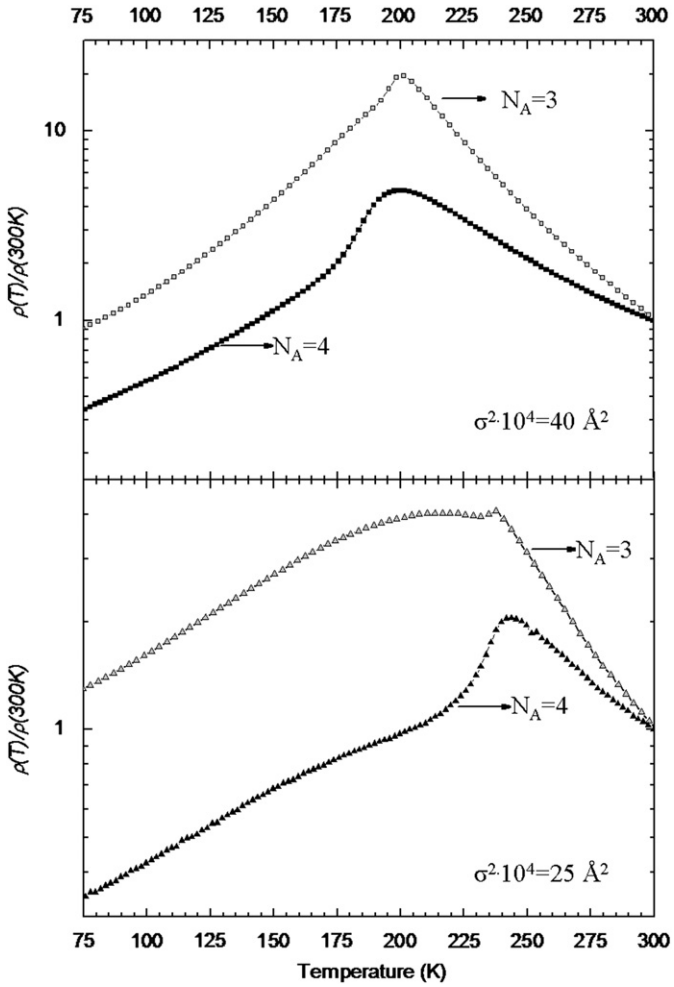

Fig. 3. RT-normalized resistivity versus temperature curves (cooling and heating cycle) for compositions with $\sigma^2 = 0.0040$ (top) and $\sigma^2 = 0.0025$ Å^2 (bottom). The $\sigma^2 \times 10^4/Å^2$ values and the number of the *A*-site cations are labeled.

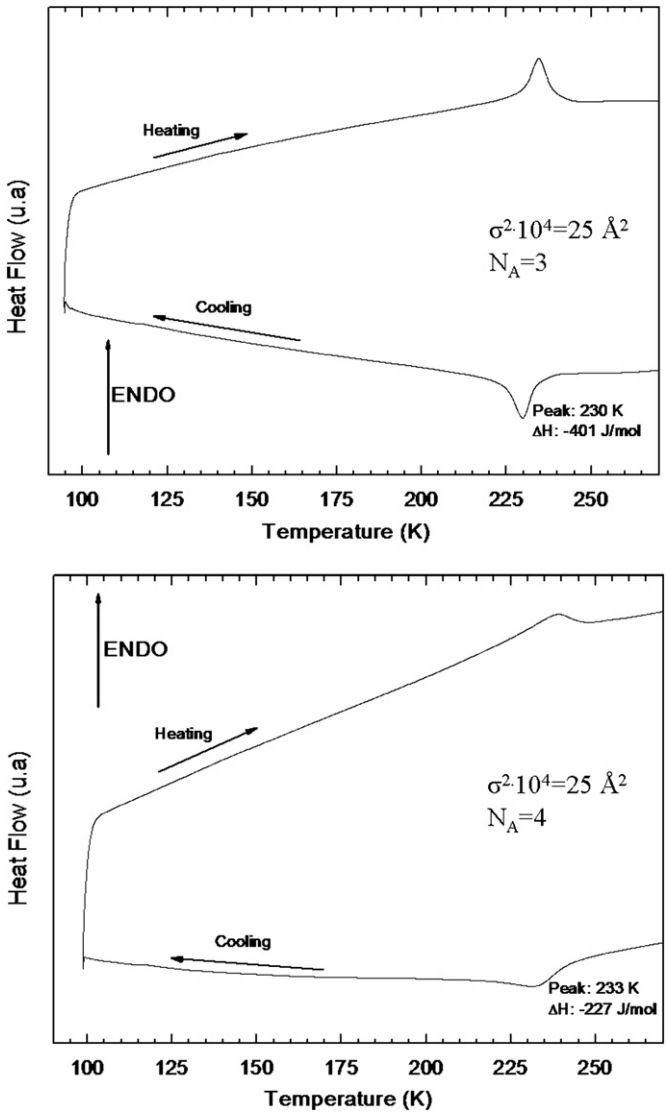

Fig. 4. DSC versus temperature curves (cooling and heating cycle) for compositions with $\sigma^2=0.0025\,\text{Å}^2$; $N_A=3$ (top) and $N_A=4$ (bottom).

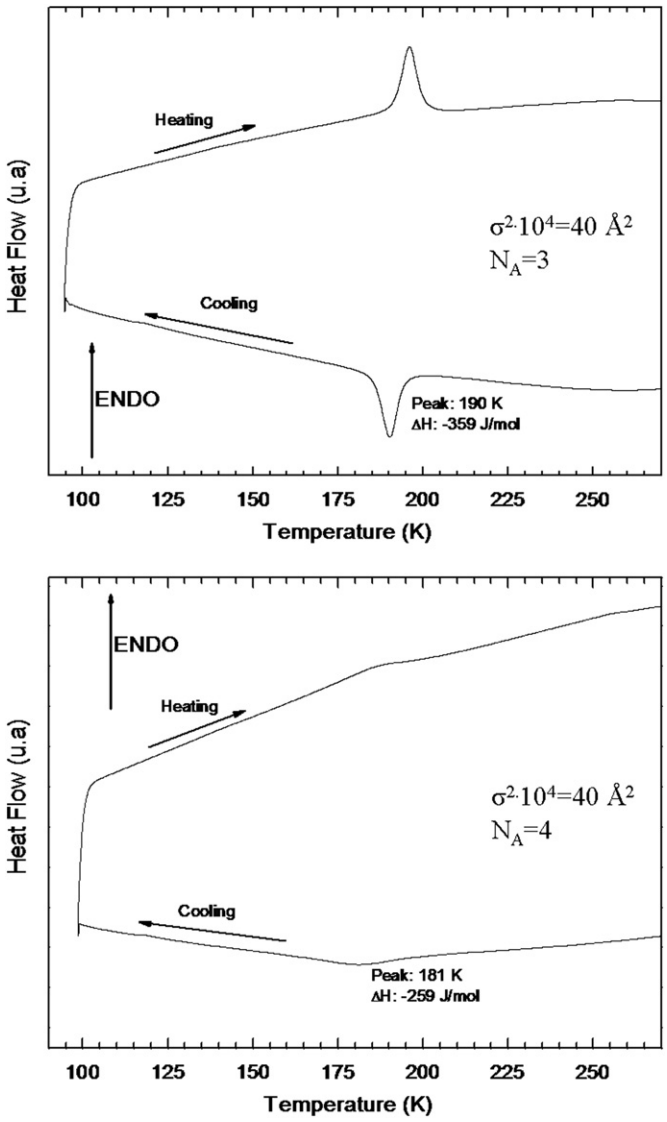

Fig. 5. DSC versus temperature curves (cooling and heating cycle) for compositions with $\sigma^2=0.0040\,\text{Å}^2$; $N_A=3$ (top) and $N_A=4$ (bottom).

values of these transitions are also given in Table 1 (values obtained on heating). For the estimation of ΔS, we consider that the two phases at both sides of the transition have the same Gibbs free energy at T_C ($\Delta S=\Delta H/T_C$).

3.5. Low-temperature thermodiffractometries

A low-temperature X-ray powder diffraction study has been carried out in order to determine if phase separation takes place below the transition temperature for most complex compositions. Fig. 7 shows the powder thermodiffractometries for $La_{0.26}Nd_{0.37}Ca_{0.23}Sr_{0.15}MnO_3$ ($\langle r_A\rangle=1.205$ Å, $\sigma^2=0.0025\,\text{Å}^2$) and $La_{0.32}Sm_{0.31}Ca_{0.18}Sr_{0.2}MnO_3$ ($\langle r_A\rangle=1.204$ Å, $\sigma^2=0.0040\,\text{Å}^2$). Similar data for $\sigma^2=0.0062\,\text{Å}^2$ ($N_A=3$) sample were recorded but they are not reported as their behaviors are similar. We did not observe signs of phase segregation in any of the compositions shown in Table 1. For the sake of comparison, the same type of data taken with identical experimental setup is also shown for $La_{0.28}Pr_{0.35}Ca_{3/8}MnO_3$ ($\langle r_A\rangle=1.191$ Å and $\sigma^2=0.0002\,\text{Å}^2$). This sample was synthesized as previously reported [12] and it is considered an archetype of spontaneous phase separation due to the appearance of inhomogeneous charge and orbital ordering on cooling [11].

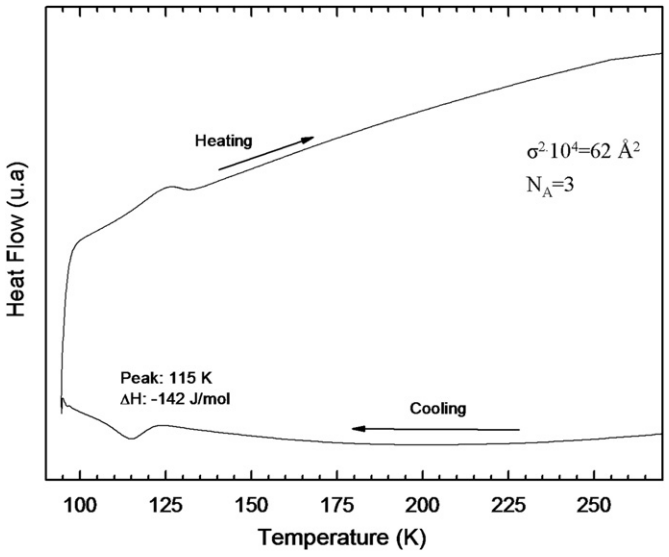

Fig. 6. DSC versus temperature curves (cooling and heating cycle) for composition with $\sigma^2=0.0062\,\text{Å}^2$, $N_A=3$.

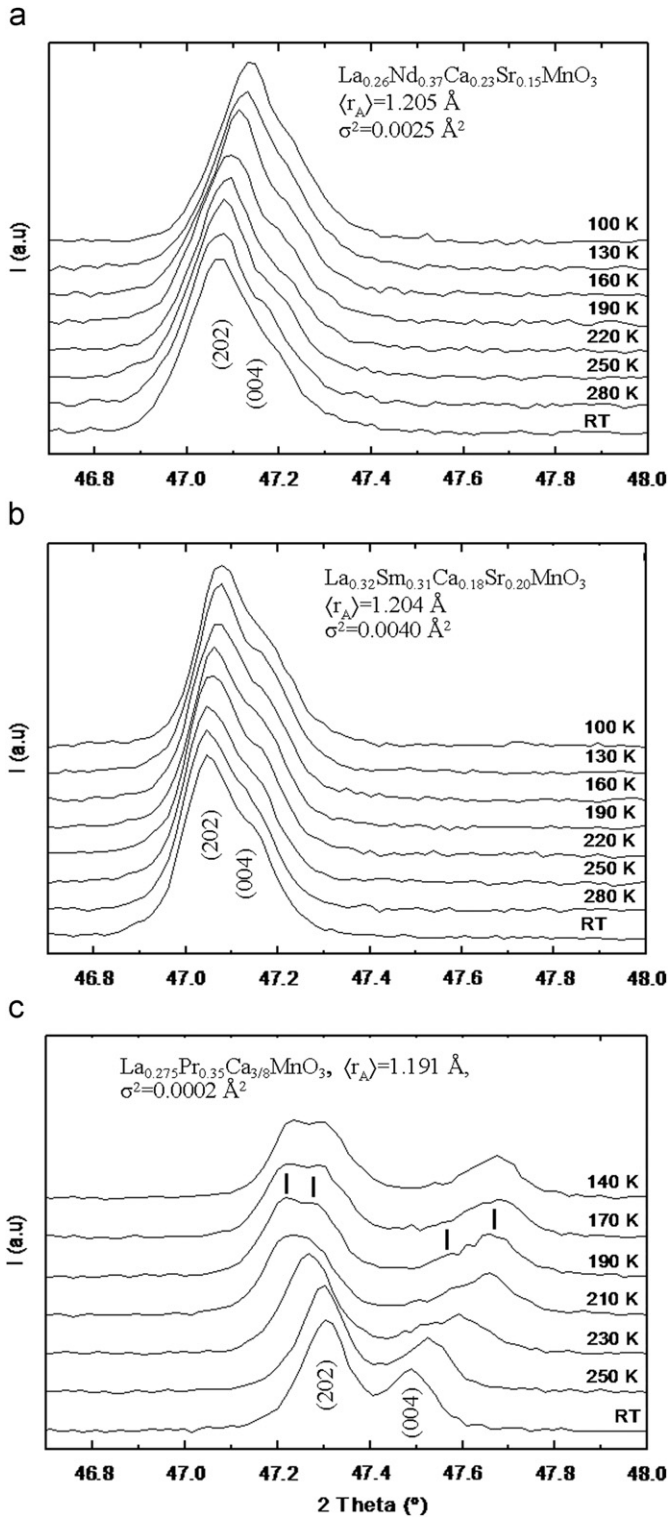

Fig. 7. Selected region of the low-temperature powder thermodiffractometries for three $Ln_{5/8}M_{3/8}MnO_3$ compositions: (a) $La_{0.26}Nd_{0.37}Ca_{0.23}Sr_{0.15}MnO_3$, (b) $La_{0.32}Sm_{0.31}Ca_{0.18}Sr_{0.2}MnO_3$ and (c) $La_{0.28}Pr_{0.35}Ca_{3/8}MnO_3$.

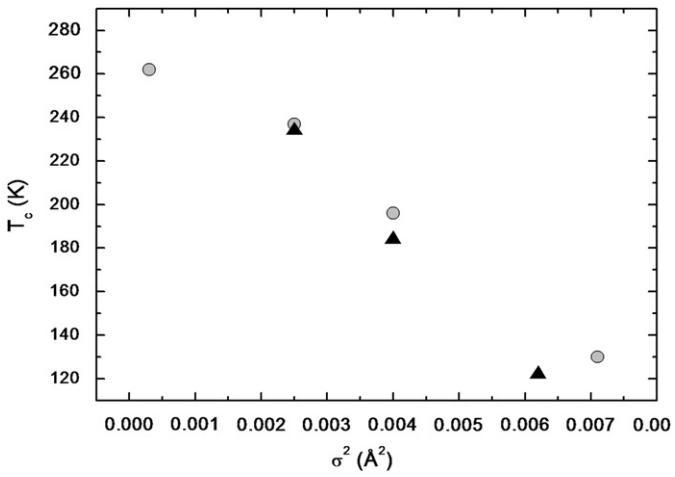

Fig. 8. T_C, obtained from the fits of one Lorentzian function to the d(M/H)/dT data, versus σ^2. The black triangles are the new compositions synthesized in this work. Gray circles correspond to data reported in Ref. [29].

4. Discussion

Regarding T_C, there is no important difference in the values of T_C of samples with the same set of x, $\langle r_A \rangle$ and σ^2 values, despite different numbers of cation species at the A site (N_A). The three new samples show the expected values for the FM–PM transition. Fig. 8 shows the evolution of T_C with σ^2 for all the samples. Therefore we must conclude that, for the same values of x, $\langle r_A \rangle$ and σ^2, N_A does not have a substantial incidence in the Curie temperature T_C as defined in Section 3.2. Their values decrease systematically with variance as previously reported [21,22,29]. Moreover, the evolution of T_{MI} along the studied series is similar to that of T_C. The deviations between samples with three or four A-site cations are lower than 10 K. However, it is of interest to note that, according to the resistivity measurements plotted in Fig. 3, samples with $N_A=3$ are clearly more resistive below room temperature than those with $N_A=4$ (for the same value of the variance). Namely, keeping the same x, $\langle r_A \rangle$ and σ^2 values, the resistivity of the studied manganites decreases when N_A increases. Such a variation suggests that the increase of chemical inhomogeneity in these samples favors formation of less resistive percolative pathways (see discussion below).

On the other hand, Fig. 2 clearly shows that samples with the same variance and $N_A=4$ have much broader magnetic transitions than those with $N_A=3$. This effect has been quantified by measuring the full width at half maximum of the derivative curves, d(M/H)/dT. The resulting values are given in Table 1. This extra broadening of the transition is also apparent in the DSC measurements (see Figs. 4–6). The extra broadening of the transition with N_A will be discussed in detail below. Moreover, the ΔH values are significantly smaller for samples with $N_A=4$ than for samples with the same variance and $N_A=3$, even after taking into account that the errors are larger for samples with $N_A=4$ since the transitions are broader. These observations indicate that, even in samples prepared with great care to minimize avoidable inhomogeneities, in these manganites, sample inhomogeneity is found to increase with N_A, as discussed in more detail below.

It must be highlighted that samples with $N_A=4$ are chemically more heterogeneous than those with $N_A=3$, although they have the same x, $\langle r_A \rangle$ and σ^2 values. We previously reported [29] that samples with $N_A=3$ did not show any evidence of phase separation as evidenced by powder X-ray thermodiffractometry. Fig. 7 shows the low-temperature patterns for $N_A=4$ samples with $\sigma^2=0.0025$ and 0.0040 Å^2. The only observed effect is the thermal contraction on cooling. Therefore, we can rule out the possibility of mesoscopic phase separation due to chemical heterogeneity in these samples. For the sake of comparison, in Fig. 7 we have included similar thermodiffraction data for $La_{0.28}Pr_{0.35}Ca_{3/8}MnO_3$, which has a slightly smaller average ionic radius ($\langle r_A \rangle = 1.191$ Å). This compound has been previously

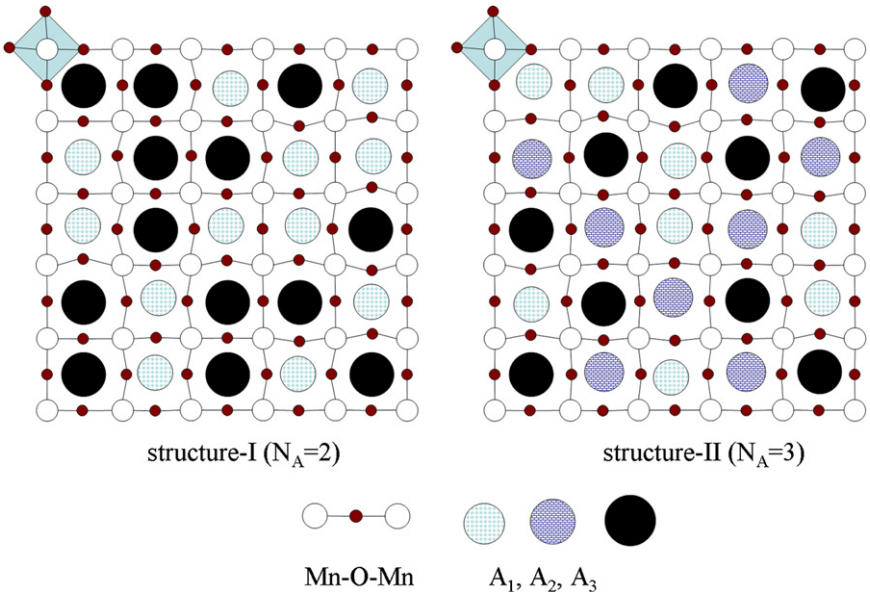

Fig. 9. Two-dimensional schematic drawing showing projections for two perovskite structures described in the text.

shown to display phase separation at the mesoscopic scale, due to the segregation of two types of cells below ~230 K [11], with the coexistence of ferromagnetic (metallic) and antiferromagnetic (charge ordered) regions of sizes close to a micrometer. This phase coexistence at low temperature can be simply evidenced by laboratory X-ray powder diffraction. For $La_{0.28}Pr_{0.35}Ca_{3/8}MnO_3$ Fig. 7(c) shows at least four diffraction peaks coming from two segregated phases (monoclinic and orthorhombic). The quantification of different phases in this system and their temperature dependence from synchrotron X-ray powder diffraction measurements will be reported elsewhere [30]. We can thus confirm that, for the samples listed in Table 1 (with $\langle r_A \rangle = 1.20$ Å and a doping level of 3/8) mesoscopic phase separation does not take place in spite of the remarkable chemical heterogeneity of some compositions.

Next, we will focus on the observed increase in width of $M(T)$, $\rho(T)$ and DSC transitions associated with larger N_A numbers, in compositions having the same x, $\langle r_A \rangle$ and σ^2 values. To interpret this result, we have to pay special attention to the modification of the manganese local environments due to an increase of N_A cations. At this point we remind that the strength of the ferromagnetic coupling J_F (double exchange), the facility of the e_g electrons to move is based on easy movement of these electrons along the oxygen bridges (Mn–O–Mn) that connect manganese atoms along the three spatial directions. The distortion of this link ($\theta \neq 180^\circ$) is locally controlled by the size of adjacent A cations. Moreover, any particular Mn–O–Mn bond angle (θ) can be assimilated to a potential energy barrier (Ω) that e_g electrons have to overcome. In other words, any particular Mn–O–Mn bond angle with exceptionally large bending certainly represents a 'bottleneck' or a barrier. The outer electrons will find a much higher potential barrier through that particular bridge and will try to search less resistive paths along other oxygen bridges.

A perovskite *Pnma* structure with a unique type of A cation presents two distinct Mn–O–Mn bond angles (θ_{ac} and θ_b). These bond angles act as bridges, but they can be considered as a barrier when a particular angle is highly distorted. Keeping the average ionic radius, $\langle r_A \rangle$, in the lattice but increasing the variance of A cations (σ^2) makes the distribution $\{\theta_i, f_i\}_{i=1\rightarrow j}$ wider in θ values around the mean angle $< \theta_i$ (j: number of dissimilar Mn–O–Mn angles; f_i: frequency of θ_i in the lattice). Moreover, to a set of angles $\{\theta_i\}_{i=1\rightarrow j}$ we can associate the corresponding set of ferromagnetic couplings $\{J_{Fi}\}_{i=1\rightarrow j}$ and of energy barriers $\{\Omega_i\}_{i=1\rightarrow j}$. In addition, a given width (variance) of the set of angles $\{\theta_i, f_i\}_{i=1\rightarrow j}$ can be obtained using a different number 'j' of distinct angles (where j is related to N_A). This description is schematically represented in Fig. 9. Structure I contains two types of A cations ($N_A=2$) whereas structure II contains three types ($N_A=3$). These hypothetical structures have suitable stoichiometries to have the same doping level x, average ionic radius $\langle r_A \rangle$ and variance σ^2.

At this point two distinct scenarios can be considered. In scenario 1, the increase in the width of the transitions is due to larger Mn–O–Mn angle variability (structure II has greater Mn–O–Mn angle variability than structure I). This implies the assumption that σ^2 is spatially homogeneous at the microscopic scale and that increasing the number 'j' in $\{\theta_i, f_i\}_{i=1\rightarrow j}$ as N_A increases produces wider transitions. However, this explanation would give rise to wrong conclusions that are in contradiction with previously reported experiments [22–29]; e.g. the variance trends previously reported work very well also for small N_A values ($N_A=2,3$) without revealing deviations due to changes in the number 'j'. No direct correspondence is seen between 'j' and the properties depending on the variance (like T_C). In this interpretation greater differences would be found between manganites with small N_A values and those matching better the continuous cation size distribution approximation to the variance for larger N_A values.

There is an alternative interpretation (scenario 2). In this second scenario, we assume that the samples may present an inhomogeneous spatial distribution of the variance $\{\sigma_I^2\}$ at the microscopic scale. Increasing N_A, real samples very likely present local variations of the variance due to statistical reasons (assuming a random distribution of the A cations in the material). Similar statistical effects in "perfectly prepared" manganites were analyzed and demonstrated [31] using Monte Carlo simulations for the coexistence of different cations at the B site [31]. Hence, the presence of such chemical inhomogeneities is not necessarily related to deficiencies in the preparation method as N_A increases (extrinsic effect), but they may be the result of statistical fluctuations (intrinsic). As a result, the samples investigated here exhibit the same mean value of the variance $\sigma \equiv \langle \sigma_I^2 \rangle$, but very likely they also present a wider distribution of σ_I^2 values at the microscopic range as N_A increases.

In conclusion, we have shown that N_A has a strong influence on the width of the ferromagnetic and metal–insulator transition, and a very small influence on the average transition temperature. This has been found by comparing different $Ln_{5/8}M_{3/8}MnO_3$ manganites with the same x, $\langle r_A \rangle$ and σ^2 values. We recall that the opposite behavior had been previously demonstrated for increasing values of the variance σ^2 in manganites with the same x and $\langle r_A \rangle$ (strong influence on T_C and small influence on the width of the transition). We attribute the N_A effects reported here to a statistical increase of spatial inhomogeneities of the variance (chemical sample inhomogeneities) for samples with larger values.

Acknowledgments

Financial supports from MICINN (Spanish government) Research Grants MAT2006-11080 and NANOSELECT CSD2007-00041, and from Generalitat de Catalunya (2009 SGR 126) are acknowledged. The FAME European Network of Excellence is also thanked.

References

[1] C.N.R. Rao, B. Raveau (Eds.), Colossal Magnetoresistance, Charge Ordering and Related Properties of Manganese Oxides, World Scientific, Singapore, 1998.
[2] Y. Tokura (Ed.), Colossal Magnetoresistive Oxides, Gordon & Breach Science, New York, 2000.
[3] S. Jin, T.H. Tiefel, M. McCormack, R.A. Fastnacht, L. Schultz, K. Samwer, Science 264 (1994) 413.
[4] For two reviews see: E. Dagatto, T. Hotta, A. Moreo, Phys. Rep. 1 (2001) 344; N.D. Mathur, P.B. Littlewood, Solid State Commun. 119 (2001) 271.
[5] A. Moreo, S. Yunoki, E. Dagotto, Science 283 (1999) 2034.
[6] A. Moreo, M. Mair, A. Feiguin, S. Yunoki, E. Dagotto, Phys. Rev. Lett. 84 (2000) 5568.
[7] A. Urushibara, Y. Moritomo, T. Arima, A. Asamitsu, G. Kido, Y. Tokura, Phys. Rev. B 51 (1995) 103.
[8] Y. Moritomo, T. Akimoto, A. Nakamura, K. Ohayama, M. Ohashi, Phys. Rev. B 58 (1998) 5544.
[9] G.H. Jonker, J.H. Van Santen, Physica (Utrech) 16 (1950) 337.
[10] P. Schiffer, A.P. Ramirez, W. Bao, S.W. Cheong, Phys. Rev. Lett. 75 (1995) 3336.
[11] M. Uehara, S. Mori, C.H. Chen, S.W. Cheong, Nature 399 (1999) 560.
[12] J.A. Collado, C. Frontera, J.L. García-Muñoz, C. Ritter, M. Brunelli, M.A.G. Aranda, Chem. Mater. 15 (2003) 167.
[13] K.H. Kim, M. Uehara, C. Hess, P.A. Sharma, Phys. Rev. Lett. 84 (2000) 2961.
[14] V. Kiryukhin, B.G. Kim, S.W. Cheong, T.Y. Hoo, J.P. Hill, I. Moon, Y.H. Jeong, Phys. Rev. B 63 (2000) 024420.
[15] H.Y. Hwang, S.W. Cheong, P.G. Radaelli, M. Marezio, B. Batlogg, Phys. Rev. Lett. 75 (1995) 914.
[16] F. Millange, V. Caignaert, G. Mather, E. Suard, B. Raveau, J. Solid State Chem. 127 (1996) 131.
[17] V. Caignaert, E. Suard, S. Maignan, C.H. Simon, B. Raveau, J. Magn. Magn. Mater. 153 (1996) L260.
[18] P.G. Radaelli, G. Iannone, M. Marezio, H.Y. Hwang, S.W. Cheong, J.D. Jorgensen, D.N. Argyriou, Phys. Rev. B 56 (1997) 8265.
[19] C.N.R. Rao, P.N. Santhosh, R.S. Singh, A. Arulraj, J. Solid State Chem. 135 (1998) 169.
[20] A.M. Balagurov, V.Y. Pomjakashin, D.V. Sheptyakov, V.L. Aksenov, P. Fisher, L. Keller, O.Y. Gorbenko, A.R. Kaul, N.A. Babuskina, Phys. Rev. B 64 (2001) 024420.
[21] J.P. Attfield, Cryst. Eng. 5 (2002) 427.
[22] L.M. Rodríguez Martínez, J.P. Attfield, Phys. Rev. B 54 (1996) R15622.
[23] L.M. Rodríguez Martínez, J.P. Attfield, Phys. Rev. B 63 (2000) 24424.
[24] J.P. Chapman, J.P. Attfield, L.M. Rodríguez Martínez, L. Lezama, T. Rojo, Dalton Trans. (2004) 3026.
[25] M.M. Seikh, L. Sudheendra, C.N.R. Rao, Solid State Sci. 6 (2004) 561–564.
[26] G. Venkataiah, V. Prasad, P.V. Reddy, J. Alloys Compd. 429 (2007) 1.
[27] D. Zhu, X.n. Tan, P. Cao, F. Jia, X. Ma, Y. Lu, J. Appl. Phys. 105 (2009) 063914.
[28] D.C. Krishna, P.V. Reddy, J. Alloys Compd. 479 (2009) 661.
[29] J.A. Collado, C. Frontera, J.L. Garcia-Munoz, M.A.G. Aranda, J. Solid State Chem. 178 (2005) 1949.
[30] J.A. Collado, J.L. García-Muñoz, M.A.G. Aranda, Manuscript in preparation.
[31] C. Frontera, J.L. García-Muñoz, Europhys. Lett. 84 (2008) 67011.